Available online at www.sciencedirect.com

SciVerse ScienceDirect

Procedia IUTAM 3 (2012) 157 – 171

Procedia IUTAM

www.elsevier.com/locate/procedia

Symposium on Linking Scales in Computations: from Microstructure to Macro-scale Properties

Advances in Multiscale modeling and characterization of granular matter

Carlos Avila[a], José Andrade[a,]*

[a]*Applied Mechanics, California Institute of Technology, Pasadena, CA 91125, USA*

Abstract

In this paper we report some key advances in the characterization and modelling of granular matter. Recent developments on experimental and imaging techniques (X-ray CT, 3D-DIC) are allowing modellers to leverage the rich information encoded at subscales that are inherent to sands and other geologic and granular materials. One of the major outcomes from these joint efforts is the development of novel multiscale computational frameworks that are able to bypass phenomenological laws by extracting fundamental sets of information at lower scales that are then used to enrich continuum plasticity models embedded in finite element codes. The effectiveness of one of these promising techniques is showcased by two examples: one linking discrete element computations with finite elements and another example linking a triaxial compression experiment using computed tomography and digital image correlation with finite element computation. In both cases, dilatancy and friction are used as a fundamental set of information and are obtained directly from grain kinematics. The results show three-dimensional multiscale results in the post-bifurcation regime with real materials and good quantitative agreement with experiments for the very first time.

.

Keywords: Multiscale; X-ray CT, Granular matter

* Corresponding author. Tel.: +1-626-395-4141; fax: +1-626-568-2719.
E-mail address: jandrade@caltech.edu (Andrade J.E.).

 doi:10.1016/j.piutam.2012.03.011

1. Introduction

1.1. Multiscale methods in mechanics

Multiscale methods generally imply the utilization of information at one length scale to subsequently model the response of the material at larger length scales [1]. Multiscale methods have emerged lately in mechanics to bridge different material scales ranging from atomic scale to continuum scale. These methods aim at obtaining constitutive responses at the continuum scale, without resorting to phenomenology. The pioneering quasi-continuum method proposed the use of the so-called Cauchy–Born rule to obtain a continuum energy density function from molecular dynamics computations within a finite region of interest [2]. Very recently, a FE^2 algorithm was proposed to aggregate discontinuities across scales in highly distorted areas in solids [3].

In the area of geomechanics, some efforts are being made to obtain more realistic models based on a multiscale philosophy, see, for example, [4;5]. At this point, techniques linking the granular and continuum scales are dependent on homogenization theory [6;5]. Recently, a new multiscale technique has been proposed to update plastic internal variables in continuum plasticity models based on micro-mechanical calculations at the cell level, without resorting to phenomenological hardening [7;8]. However, there are still fundamental questions that need to be addressed to better understand and model the mechanics and physics of granular matter across scales.

1.2. Multiscale nature of granular matter

Granular matter is ubiquitous in nature and engineering and appears in a plethora of presentations including sands, sandstones, concrete, pharmaceutical pills, and nanoparticles, just to name a few. In order to understand and predict the behavior of granular materials, one must recognize that their macro mechanical behavior is fundamentally encoded at the granular scale.

Recent developments on experimental and imaging techniques combined with novel multiscale computational frameworks are expanding the frontiers of our understanding of the physics driving the response of granular matter at different subscales and subsequently allowing us to better predict the macro structural response of these type of materials.

In the context of granular materials this emerging multiscale modeling philosophy leave us with two fundamental questions:

1. What is the fundamental set of information to be passed between scales in a discrete-continuum material?
2. What is the role of micro-structure in the determination of material behavior at the continuum level?

To begin answering these questions, current numerical techniques such as the finite element method (FEM) [10;11] and the discrete element method (DEM) [12] together with novel experimental and imaging techniques (X-ray CT, 3D DIC) are exploited and furnished into a new class of numerical algorithms. These new algorithms that are proving to be more accurate, even in regions where current models used independently fail either due to their phenomenological nature in the case of FEM [13;14;15;16;17;18;19;20;21;22;23] or due to high computational costs and, related to this, inability to capture salient features of granular materials such as complex shape and associated interparticle contact characteristics in the case of DEM [24;25; 26;27].

The first question above is pertinent to all multiscale methods and is vital to faithfully capture micro-mechanical behavior. The second question pertains to accurate modeling of real materials, since in the case of real sands and other geologic materials, grain shape and definition of contact characteristic play a central role in influencing macroscopic mechanical response [23].

The novel hierarchical scheme described in the following sections exploit the ability of DEM and experiments to capture the kinematics of grains and extracts from these information the frictional resistance and dilatancy, which are known to be key variables in the macroscopic description of granular materials [28;29]. The coupling with computations helps us show that these two parameters are sufficient to describe the macroscopic behavior of the underlying granular model (hence answer the first question above). In the case of DEM computations the predictions by the multiscale scheme are only as accurate as the underlying discrete model turning this —at least for the moment— in a validation process for the multiscale methodology.

To furnish a validation process, the multiscale technique uses advanced experimental data obtained at the European Synchrotron Radiation Facility (ESRF). These rich experimental data, allow us to characterize the grain kinematics of real sands while sheared under axisymmetric compression [30]. From these data, we also extract dilatancy and friction (using a stress-dilatancy relation) evolutions amenable to these recently developed multiscale method. A persistent shear band appearing in the experiment is modeled accurately by invoking the multiscale technique within a finite element framework. Clearly current micro-mechanical models have difficulties capturing complex behavior of real granular materials such as sands, with some progress made by recently proposed models [31;32]. Nevertheless, the multiscale model is able to leverage the rich data obtained from the experiments and capture the kinematics and macroscopic response implied by the persistent shear band in three dimensions for the first time. This example sheds light into answering the second question above and opens the door to developing more powerful models that rely on physics rather than phenomenology for granular matter.

The paper is organized in three parts: Introduction, multiscale nature of granular material, multiscale framework, and representative multiscale computations. The multiscale framework describes the classic continuum elastoplastic model for granular matter, depicting clearly the role of the plastic internal variables friction and dilatancy. Also, the micro-mechanical description is furnished in this section by the discrete element method and grain kinematics obtained from experimental data using X-ray computed tomography and digital image correlation. Coupling approaches are introduced at the end of this section. Representative multiscale computations using both discrete element method and experimental data are shown next.

Nomenclature: Bold-faced letters denote tensors and vectors; the symbol '.' Denotes an inner product of two vectors (e.g., $\mathbf{a.b} = a_i b_i$) or a single contraction of adjacent indices of two tensors (e.g., $\mathbf{c.d} = c_{ij} d_{jk}$); the symbol ':' denotes an inner product of two second-order tensors (e.g., $c{:}d = c_{ij} d_{ij}$) or a double contraction of adjacent indices of tensors of rank two and higher (e.g., $\mathbf{C{:}\varepsilon}^e = C_{ijkl} \varepsilon^e_{kl}$); the symbol '$\otimes$' denotes a juxtaposition, e.g., $(\mathbf{a}\otimes\mathbf{b})_{ij} = a_i b_j$. Finally, for any symmetric second order tensor α and β, $(\alpha\otimes\beta)_{ijkl} = \alpha_{ij}\beta_{kl}$, $(\alpha\oplus\beta)_{ijkl} = \alpha_{ik}\beta_{jl}$.

2. Describing granular materials at different scales

2.1. Continuum scale: Elastoplasticity

Consider the classical two-invariant linear elastic–plastic Drucker-Prager model. Within this context, the strain rate is split into elastic and plastic components by the additive decomposition assumption

$$\dot{\boldsymbol{\varepsilon}} = \dot{\boldsymbol{\varepsilon}}^e + \dot{\boldsymbol{\varepsilon}}^p \tag{1}$$

The inelastic response is encapsulated in the yield surface and plastic potential given by the first two invariants of the stress tensor namely,

$$p = \frac{1}{3} tr\boldsymbol{\sigma} \text{ and } q = \sqrt{\frac{3}{2}} \|dev\, \boldsymbol{\sigma}\| \tag{2}$$

with $tr\blacksquare = \blacksquare : \delta$ and $\text{dev}\blacksquare = \blacksquare - {}^{1}/_{3}\,(tr\blacksquare)\,\delta$ as the trace and deviatoric operators for a second order tensor, respectively, and $\|\blacksquare\| = \sqrt{\blacksquare : \blacksquare}$ as the L2-norm for a second-order tensor. Usually, p is referred to as the mean stress and q as the deviatoric stress, thus describing independent invariants of the stress tensor.
Using the aforementioned invariants of the stress tensor, the yield surface and plastic potential for a Drucker–Prager-type nonassociative model for cohesionless materials can be postulated, i.e.,

$$F(p, q, \mu) = q + \mu p = 0 \tag{3}$$

$$Q(p, q, \beta) = q + \beta p - \bar{c} \tag{4}$$

With μ typically referred to as the generalized friction coefficient, β is the plastic dilatancy, and $\bar{c}$ is a free parameter so that the plastic potential crosses the yield surface at the same stress state (p, q). Fig. 1 shows a schematic of the yield surface and plastic potential and the geometric meaning for the plastic internal variables (PIVs): μ, β, and $\bar{c}$. The nonassociative flow rule is given in the classic form with the direction of the plastic strain rate determined by the normal to the plastic potential so that:

$$\dot{\boldsymbol{\varepsilon}}^p = \dot{\lambda}\boldsymbol{q} \tag{5}$$

With $\boldsymbol{q} = {}^{\partial Q}/_{\partial \boldsymbol{\sigma}}$. The scalar $\dot{\lambda}$ is called the consistency parameter and controls the magnitude of plastic strain rate. Similarly, one can define the first two invariants for the strain rate tensor $\dot{\boldsymbol{\varepsilon}}$ so that:

$$\dot{\varepsilon}_v = tr\, \dot{\boldsymbol{\varepsilon}} \text{ and } \dot{\varepsilon}_s = \sqrt{\frac{3}{2}} \|dev\, \dot{\boldsymbol{\varepsilon}}\| \tag{6}$$

Using these definitions for the strain rate invariants and the particular form for $\boldsymbol{q}$ emanating from the Drucker–Prager model, one can obtain that

$$\dot{\varepsilon}_v^p = \dot{\lambda}\beta, \qquad \dot{\varepsilon}_s^p = \dot{\lambda}, \qquad \beta = \frac{\dot{\varepsilon}_v^p}{\dot{\varepsilon}_s^p} \tag{7}$$

where it is clear that the plastic dilatancy β controls the volumetric plastic strain rate for a given

deviatoric strain rate.
The canonical elastic perfectly plastic continuum tangent—relating the change in total strain to the change in stress—is then obtained by the generalized Hooke's law, the nonassociative flow rule, and the consistency condition at flow ($\dot{F} = 0$), so that

$$\boldsymbol{C}^{ep} = \boldsymbol{C}^{e} - \frac{1}{\chi}\boldsymbol{C}^{e}:\boldsymbol{q} \otimes \boldsymbol{f}:\boldsymbol{C}^{e}, \text{ where: } \chi = \boldsymbol{q}:\boldsymbol{C}^{e}:\boldsymbol{f} \tag{8}$$

In the special case of the Drucker–Prager-type plasticity model considered herein, the gradient to the yield surface, $\boldsymbol{f} = {}^{\partial F}/_{\partial \boldsymbol{\sigma}}$, and the gradient to the plastic potential $\boldsymbol{q} = {}^{\partial Q}/_{\partial \boldsymbol{\sigma}}$ take the special form

$$\boldsymbol{f} = \frac{1}{3}\mu\boldsymbol{\delta} + \sqrt{\frac{3}{2}}\hat{\boldsymbol{n}} \tag{9}$$

$$\boldsymbol{q} = \frac{1}{3}\beta\boldsymbol{\delta} + \sqrt{\frac{3}{2}}\hat{\boldsymbol{n}} \tag{10}$$

Where: $\hat{\boldsymbol{n}} = {}^{dev\,\boldsymbol{\sigma}}/_{\|dev\,\boldsymbol{\sigma}\|}$ is a unit tensor coaxial with the deviatoric component of the stress tensor.

Remark 1. The elastoplastic tangent in Eq. (8) is identical to that of a perfectly plastic model. The reason for this is that the PIVs in this multiscale plasticity model are frozen within loading increments [7]. However, the PIVs are allowed to update between loading increments. The evolution of the PIVs is obtained from the microstructure, rather than a hardening law, and can be considered piecewise constant.
The plastic internal variables (PIVs) in this model are the frictional resistance μ and the plastic dilatancy β. Typically, the value of the PIVs have to be prescribed a priori or their evolution is tied to some kind of phenomenological hardening law. However, in this paper, we propose the evaluation of the PIVs directly from the microstructure, using multiscale analysis. The micro-structural information will be provided either by discrete element method (DEM) calculations (e.g., Section 3.2) or detailed experiments (e.g., Section 4.1).

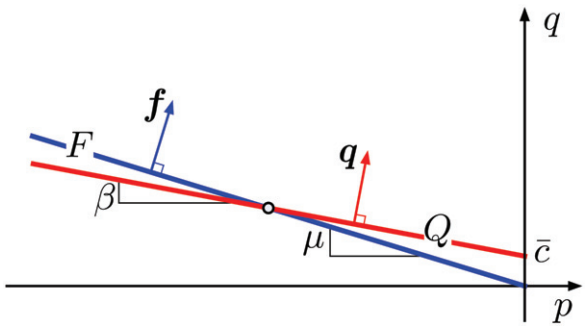

Fig. 1. Geometric attributes for Drucker–Prager-like model.

2.2. Grain scale: DEM and advanced experimental techniques

2.2.1 DEM models

As mentioned before, the most basic physical phenomena in granular media are encoded in the grain scale. Based on this premise, many efforts have been made to advance the state of the art in discrete

mechanics. The discrete element method (DEM) developed by Cundall and Strack [12] to account for the inherently discontinuous and heterogeneous nature of granular materials, in principle, relies solely on the satisfaction of basic Newtonian mechanics. The idea was to replace the continuum mechanics formulation plagued by phenomenology and, in the case of rate independent models, pathological mesh dependence post-peak. However, computational expenses have crippled discrete mechanics methods, which are not yet able to resolve the grain scale accurately and have had to resort to the same techniques required to calibrate phenomenological models [27]. It is not uncommon to use 'grains' of much larger size or mass in order to simulate field scale problems under quasi-static conditions. It is expected that discrete mechanics methods will not reach the ability to predict the behavior of granular systems at a specimen and field scale for the next twenty years [32;33]. However, grain scale mechanical models can certainly be used to extract meso-scale behavior, which can then be up-scaled by continuum models. Used with care, DEM enables us to examine the grain-scale mechanisms governing the macroscopic behavior of granular media under quasi-static and dynamic conditions.

2.2.2 Homogenization

It is important to define the concept of a unit cell at this point. Unlike a representative element volume (REV) the unit cell may not necessarily represent the behavior of the entire domain. However, similar to the concept of REV, the unit cell is defined as the smallest physical domain where the continuum is applicable (high frequency oscillations are not present in a given continuum quantity, e.g., dilatancy). Therefore, the unit cell is meaningful at the meso scale and above. Within a unit cell of volume V the average micro-mechanical stress $\overline{\boldsymbol{\sigma}}$ is obtained by invoking standard equilibrium conditions [35], i.e.,

$$\overline{\boldsymbol{\sigma}} = sym\left[\frac{1}{V}\sum_{n=1}^{Nc} \boldsymbol{l}^n \otimes \boldsymbol{d}^n\right] \tag{11}$$

Here $\boldsymbol{l}^n$ represents the contact force at contact point n, $\boldsymbol{d}^n$ denotes the distance vector connecting two particles in contact at n, and Nc is the total number of particles encapsulated in the volume V of the unit cell. Again, V must be large enough for Eq. (11) to be meaningful in the continuum sense. The stress response obtained from Eq. (11) comes directly from the grain scale mechanics and reflects the configuration and constitutive response of the grains themselves. It could be argued that Eq. (12) is purely physics-based and that phenomenology is not involved in its derivation. However, for reasons previously stated, the constitutive response of the granular system is typically altered in order to resolve practical problems of interest and hence Eq. (11) is reduced to a phenomenological approach. This deficiency can be eliminated if one focuses the computation to small regions such as the aforementioned unit cell.

Similar to the average micro-mechanical stress, the average micro-mechanical strain tensor $\overline{\boldsymbol{\varepsilon}}$ can be computed from the granular kinematics, specifically using the displacement field. However, the calculation of $\overline{\boldsymbol{\varepsilon}}$ is significantly more involved as it requires integration of the displacement field over the boundary of the unit cell. We introduce a discrete procedure exploiting the convex hull calculation proposed by Barber et.al. [35] to calculate surface areas using a triangular discretization so that,

$$\overline{\boldsymbol{\varepsilon}} = sym\left[\frac{1}{V}\sum_{n=1}^{N_t}(\boldsymbol{u}^n \otimes \boldsymbol{v}^n)A^n\right] \tag{12}$$

Fig. 2 shows a schematic of the triangular discretization and a close up into the main ingredients involved in the calculation. In the resulting procedure, the displacement $\boldsymbol{u}^n = \frac{1}{3}(\boldsymbol{u}^{i,n} + \boldsymbol{u}^{j,n} + \boldsymbol{u}^{k,n})$ is the average of the displacements $\boldsymbol{u}^{i,n}, \boldsymbol{u}^{j,n} and\ \boldsymbol{u}^{k,n}$associated with particles i, j and k, which define the n-th triangle. The vectors $\boldsymbol{v}^n$ define the normal and A^n is the area of the n-th triangle respectively. The dyadic products are summed over all the N_t triangles discretizing the surface area of the volume of measure V.

Using the average stress and strain measures introduced above, we can extract the current state of the particle assembly and use this information to perform multiscale computations by, for instance, extracting the PIVs introduced in Section 2.1. The multiscale procedures used to perform this extraction will be discussed in the following sections.

When used at the appropriate scale, the main advantage of the grain scale approach, exemplified by the DEM, is the ability to bypass the phenomenological approach necessitated hitherto by classical plasticity models. Its main disadvantage is the computational expense required, and related to this, the current inability to simulate complex 3D granular systems, such as natural sands. One alternative is to develop high-fidelity algorithms to capture material behavior more accurately and focus the effort on small regions.

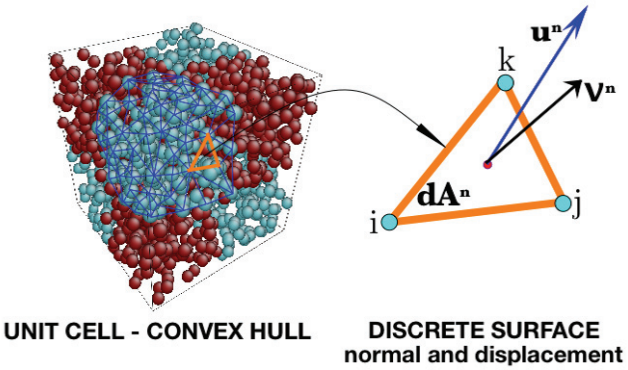

Fig. 2. Unit cell surface discretized using triangular elements defined by the centroids of particles associated with the boundary. Inset shows the n-th triangle and its associated nodes, average displacement $\boldsymbol{u}^n$, normal $\boldsymbol{v}^n$, and area A^n.

2.2.3 Grain scale imaging and 3D digital image correlation

An alternative to DEM calculations is furnished by advanced experimental techniques combined with modern imaging. In fact, X-ray computed tomography (XR-CT) and 3D digital image correlation (3D-DIC) are two techniques currently being used in concert to extract very important information from experiments. Depending on resolution, one can obtain meso scale, and even grain scale, images of the deformation in granular materials. Fig. 3 shows the grain scale configuration obtained via synchrotron XR-CT in situ (i.e., on site and in real time) during a triaxial compression experiment in dense sand. The image was obtained by researchers at the 3S-R Labs using the European Synchrotron Radiation Facility (ESRF) in Grenoble, France [34]. The observed mean grain diameter was about 300μm and the sample diameter was 11 mm. At different levels in the loading program, 3D images, such as that shown in Fig. 3 were obtained by stacking several slices. The image was obtained using X-ray CT and 3D-DIC on a sample of argillaceous sand under triaxial compression. As demonstrated in the figure, the technique allows for accurate calculation of the strain field at the meso (continuum) scale.

Either via grain scale computations (e.g., using DEM) or using advanced experimental techniques enhanced by imaging capabilities, the time is ripe to look at the micro-structure in areas of interest, for example shear bands, and probe the microstructure to obtain high-fidelity material parameters. These parameters stemming directly from the microstructure can be used at the continuum scale, perhaps in lieu of phenomenologically driven ones. The next section outlines this concept further for the class of plasticity models presented in the previous sections.

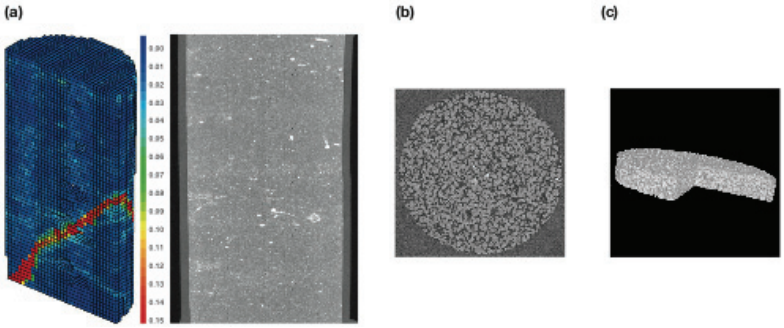

Fig. 3. (a) Deformation mapping using X-ray CT and 3D-DIC. Left (in color): deviatoric incremental strain (strain averaged over the elements: local gauge length is 280 lm); right: radiographic cut just after the peak deviator stress. After Lenoir et al. (2007). (b) Slide of sample of sand and (c) 3D reconstruction by staking slices. Original image courtesy of 3S-R Labs, Grenoble, France (For interpretation of the references to color in this figure legend, the reader is referred to the web version of this paper.)

3. Multiscale framework: from grain kinematics to continuum mechanics

3.1. Linking elastoplasticity and grain-scale kinematics

In this section, a simple multiscale framework is proposed for coupling grain scale mechanics, stemming from computations or high-fidelity experiments, with continuum plasticity models, such as those presented above. The proposed framework will make use of the concept of friction and dilatancy, parameters that will be obtained directly from the microstructure. Recall the definition for the dilatancy parameter, i.e.,

$$\beta = \frac{\dot{\varepsilon}_v^p}{\dot{\varepsilon}_s^p} \approx \frac{\dot{\varepsilon}_v}{\dot{\varepsilon}_s} \tag{13}$$

We have neglected the elastic strain increments to write the approximation with the total strain increments for the computation of dilatancy. This is a plausible approximation once plasticity dominates the deformations, which is the case for most granular materials after yielding. Therefore, the dilatancy can be extracted directly from unit cell computations or from experiments and passed directly to the plasticity model. This will eliminate the need for a phenomenological evolution law relating the dilatancy to the plastic strains. Eq. (12) gives the average strain tensor, then its invariants are computed and Eq. (13) is used to obtain dilatancy.

By the same token, the frictional resistance can be computed directly from the unit cell calculations by exploiting the average stress Eq. (12). Hence, $\mu \approx \frac{p}{q}$ can be calculated from the stress ratio obtained from the average stress $\bar{\boldsymbol{\sigma}}$ from the DEM and passed upwards to the plasticity model without resorting to a hardening law.

Unlike numerical simulations by DEM, experimental results cannot be used to extract measurement of stress (at least not yet) to approximate the value of friction. Therefore, we recur to a well-established concept in soil mechanics: a stress–dilatancy relation [28;37] expressed as: $\mu \approx \beta + \mu_{cv}$, to update the frictional resistance as a function of the dilation resistance. We will use this stress–dilatancy relation and will hence need to calculate the value of frictional resistance at constant volume μ_{cv} during the critical state or when dilatancy is all spent ($\beta = 0$).

If the dilatancy is obtained directly from the unit cell computations, and then the frictional resistance is updated via a stress–dilatancy relation, the plasticity model only requires three material constants, i.e.,

Young's modulus E, Poisson's ratio ν, and the residual frictional resistance μ_{cv} (alternatively, ϕ_{cv}). These material constants have a very clear physical interpretation and can be obtained simultaneously from just one experiment, e.g., direct shear. It is apparent that the success of the framework depends crucially on the correct extraction of the dilatancy from the unit cell computations. One important detail to keep in mind is that dilatancy in granular media is path-dependent. Therefore, compatibility of deformations and stresses between the macroscopic and microscopic model must be ensured. In other words, if the dilatancy at an instant in discrete time t_{n+1} is to be extracted (as done in finite elements or finite differences), then the deformation history encapsulated in the macroscopic strain tensor $\boldsymbol{\varepsilon}_n$ must be projected onto the unit cell. The multiscale scheme hinges on three crucial steps: 1. Imposing boundary conditions, 2. Extracting information from the micro-scale (i.e. DEM or experiments), 3. Updated continuum model as depicted in Fig. 4.

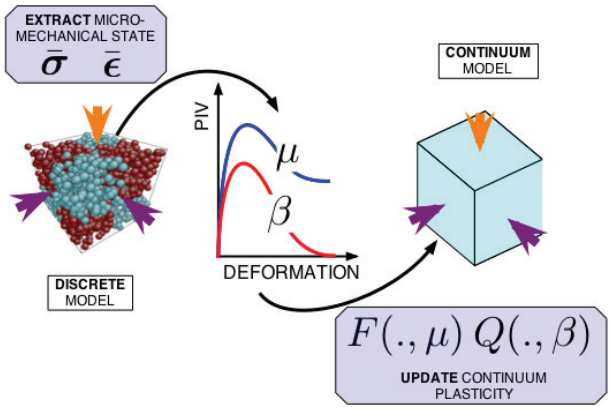

Fig. 4. Schematic showing hierarchical multiscale calculation to extract micro-mechanical state (stress and strain) and use it to obtain the evolution of the plastic internal variables (PIVs) as a function of the deformation. These PIVs are subsequently used to update the plasticity model used in continuum calculations. The discrete model could be either DEM or experiments.

3.2. Unit-cell computations: DEM-based modelling

In this section, the recipe shown in Section 3.1 is explicitly exploited to extract material behavior directly from the 3D granular assembly shown in Fig. 4a. This 3D assembly is loaded under triaxial compression and its behavior is simulated directly using the discrete element method. The results from the DEM calculations can be seen as direct numerical simulations (DNS) and, hence, the success or accuracy of the multiscale method will be judged by how well it can replicate the DNS results. Average stress and strain tensors are computed and the plastic internal variables extracted from the micro-scale are updated into the continuum plasticity model. This example showcases the ability of the method to extract material behavior on the fly. The granular assembly is consolidated to an initial packing density of 0.345 using a hydrostatic pressure of 860 kPa. After the consolidation step, the lateral walls of the sample are held at constant pressure, while the top face is moved uniformly downwards. The bottom face is not allowed to displace vertically. The stress–strain response for the DEM calculations are shown in Fig. 4b. Using identical boundary conditions, one isoparametric 'brick' element (8 displacement nodes) was used to implement the multi-scale computations using the Drucker–Prager model. Since the response is fairly homogeneous, the extracted parameters, i.e., μ and β are used in all eight Gauss points. Dilatancy and friction are extracted from the DEM code at every step in the FEM computation. The constant material parameters used in the multiscale computations are $E = 300MPa$, $\nu = 0.25$, $\eta_{cv} = 0.6$.

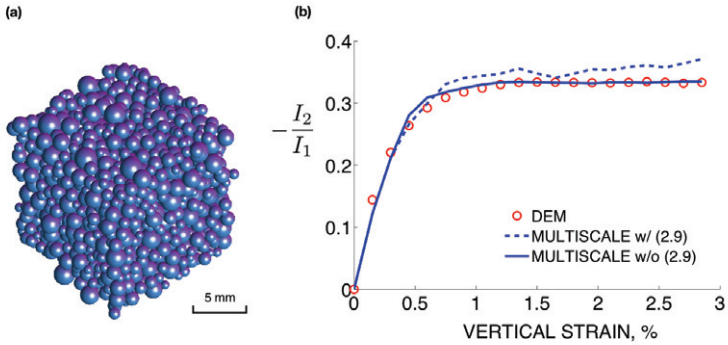

Fig. 4. (a) Initial configuration of granular assembly loaded under TXC using 3D DEM (b) Stress ratio I_2/I_1 vs. vertical strain comparing DEM and multiscale responses. The reader is referred to [7] for comparisons between the multiscale model and DEM computations.

3.3 Multi-cell computations: Experiment-based modelling

In this section, the localized incremental displacement fields of a sand specimen obtained experimentally and presented in Fig. 6a is used to perform hierarchical multiscale computations to predict the structural response of an analogous numerical sample. The idea is to link regions of the experimental sample, discretized by unit cells, with equivalent regions in a numerical sample, discretized with brick finite elements. Incremental displacements are obtained at the centroids of unit cells in the experiments and associated with a particular node in the finite element mesh. Then, strains are obtained using finite element interpolations [38], i.e.,

$$\Delta\boldsymbol{\varepsilon}^e = \boldsymbol{B}^e \Delta\boldsymbol{d}^e \tag{14}$$

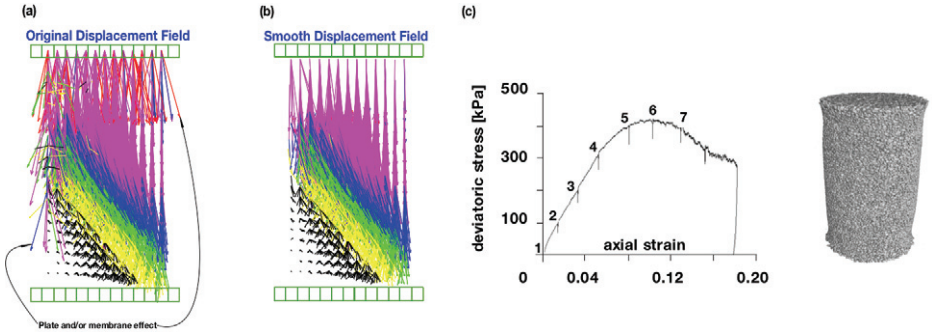

Fig. 6. Experimental Results from DIC enhanced X-ray tomography between stages 6 and 7 in (c) (post-peak response). Raw incremental displacements are shown in (a) whereas (b) shows incremental displacements after cells adjacent to the platens and membrane are removed. The figure shows a clear persistent shear band near the center of the specimen. Green cells represent top and bottom platens. (c) Global stress–strain curve and micro-structure. (For interpretation of the references to color in this figure legend, the reader is referred to the web version of this article

Where, $\Delta\boldsymbol{\varepsilon}^e$ is the incremental strain over element e, $\Delta\boldsymbol{d}^e$ is the incremental displacement vector containing the nodal incremental displacements (obtained experimentally), and $\boldsymbol{B}^e$ is the classic strain–displacement matrix, congruent with Voigt notation. Incremental strains are calculated over each Gauss integration point (eight integration points are used for the trilinear brick elements) and then used to

compute the average incremental strain over the element. The respective deviatoric and volumetric invariants are extracted from each incremental strain over each element. The multiscale model presented in Section 3.1 requires calibration of two elastic constants and the evolution of the PIVs μ and β from the micro-scale. The elastic constants can be obtained from the global load–displacement curve by making an assumption about the Poisson ratio of the material. Typical Poisson ratio ν for sands is around 0.3. Assuming this value, the shear modulus of the material can be obtained from the apparently linear portion of the deviatoric stress versus axial strain Curve shown in Fig. 6c. We assume linear elastic behaviour up to stage 4, around 0.05 axial strain. Note the sample is loaded under a constant radial stress of 100 KPa and there was no direct measure of radial strains. The estimated shear modulus of the material G comes up to be 2.6 MPa. Together, G and ν dictate the elastic behavior of the material. The frictional resistance μ is a function of the state of stress and will be inferred indirectly in this study. To approximate the value of friction, we recur to a well-established concept in soil mechanics: a stress–dilatancy relationship [29; 38]. A typical stress–dilatancy relation is given in Section 3.1. We will use this stress–dilatancy relation and will hence need to calculate the value of frictional resistance at constant volume μ_{cv} during the critical state or when dilatancy is all spent (i.e., $\beta = 0$). We assume that the value of μ_{cv} is a material constant and it is hence the same for the entire specimen. Since we have assumed that the material is linear-elastic (and homogeneous) up to loading stage 4 (up to about 0.05 axial strain in the triaxial compression experiment), we further assume that plastic deformations follow after stage 4 and that dilatancy is nil at the beginning of the plastic process. Accordingly, the residual frictional strength at that point, according to the stress–dilatancy relation, would be $\mu = \mu_{cv} = -{}^{p}/_{q}$ and, therefore, the corresponding residual strength $\mu_{cv} \approx \frac{300}{200} = 1.5$ for the entire sample.

Remark 2. The assumption of elastic deformations up to stage 4 or about 0.05 axial strain is mostly based on the apparent linear portion observed in Fig. 6c. Furthermore, this assumption facilitates greatly the modeling process. Also, it meshes well with the dilatancy (and plastic) process starting from zero, since the sample does compress during the elastic process, as expected from a relatively dense sample. Subsequent positive dilation will be responsible for the ensuing dilative process.

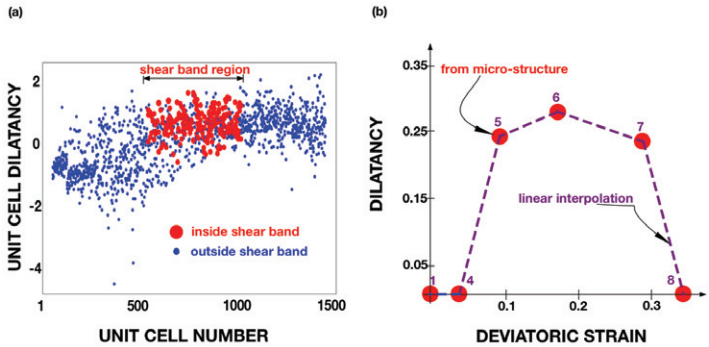

Fig. 7 (a) Dilatancy values for increment between deformation stages 6 and 7. Red dots represent values of dilatancy for elements inside the shear band and within the central portion of the sample. (b) Average dilatancy inside the shear band from incremental response such as that shown in (b). Dilatancy is assumed to be nil during the elastic regime (from stage 1 to 4) and at stage 8 (critical state is assumed). (For interpretation of the references to color in this figure legend, the reader is referred to the web version of this article.)

The central ingredient of the hierarchical multiscale model is the extraction of dilatancy β from each unit cell as a function of vertical or deviatoric strain, in order to obtain the complete evolution for the PIVs from the micro-structural process. This can be achieved using the aforementioned incremental strains stemming from the incremental displacements obtained using 3D-DIC linked to X-ray CT data (see Fig.

6b and Eq. (14)). Fig. 7a shows the values of dilatancy β calculated for every element in the sample during the incremental step between stages 6 and 7 (post-peak). As shown in Fig. 7a, we model the average evolution of dilatancy by selecting the unit cells in the central portion of the sample and those unit cells that display average shear strains above 0.15. The central portion of the sample is used to extract average material responses with as little influence from boundary effects as possible. Fig. 7b shows the resulting average dilatancy as a function of the global deviatoric strain for all unit cells inside the shear band and in the central region of the specimen. For instance, point 7 on the dilatancy curve shown in Fig. 7b is obtained by averaging the dilatancy values of those cells inside the shear band and in the central portion of the sample (red points in Fig. 7a).

Remark 3. Incremental displacements between loading stages 7 and 8 were not used for computing dilatancy values since the sample appears to buckle at or after stage 7, hence potentially affecting dilatancy values. Rather, we assumed that the dilatancy values inside the shear band at stage 8 approaches critical state ($\boldsymbol{\beta} = \mathbf{0}$). This assumption is consistent with the apparent value of deviatoric stress at that stage.

Once the average dilatancy β evolution is obtained for the elements inside the shear band, the structural response of the sample can be modeled using the hierarchical multiscale technique presented in Section 3.1. As mentioned before, trilinear brick elements were used to model the cylindrical sample. The elastic material response is assumed to be homogenous and the evolution of the PIVs is assumed to be homogeneous (inside and outside the shear band) up to loading stage 6 (peak of the stress–strain curve). This is a modeling assumption, since the 3D-DIC with X-ray CT data shows inhomogeneous responses roughly after stage 4. This assumption simplifies the modeling effort significantly, and as we will show, does not affect the results significantly. After loading stage 6, the dilatancy evolution for the elements inside the shear band is governed by the curve in Fig. 7b and for those elements outside the shear band, it is assumed to stay at the peak value (around 0.3) attained at stage 6 (this assumption is immaterial as these elements go into elastic unloading). This produces a state of inhomogeneous deformation after stage 6 (around 0.1 axial deformation), where the bulk of the deformation and the global response of the sample is governed by the evolution of the shear band.

The obtained results are quite encouraging for a variety of reasons. First, the hierarchical multiscale model is very simple, relying on a simple linear elastic response accompanied by a two-parameter plasticity model (friction and dilatancy). From these results, it seems plausible to suggest that μ and β do indeed capture the bulk of the material response, even in 'hot' areas such as shear bands. Second, these are, to the knowledge of the authors, the first multiscale results where direct comparison with experimental results has been made, at least for granular materials. Fig. 8a shows the global deviatoric stress versus the average nominal deviatoric strain of the sample computed from the hierarchical multiscale model and compared against the corresponding experimental global response. It can be seen that the stress–strain response of the numerical and physical samples agree very well. The multiscale model is able to capture the peak stress as well as the pronounced softening produced by the formation of the persisting shear band. Furthermore, the assumption of homogeneity up to the peak stress seems to be plausible, at least from a macroscopic standpoint. The deviatoric strains across the sample at loading stage 7 (about 0.13 axial strain), as calculated from the multiscale model and the experimental data, are reported in Fig. 8b. It is evident that the multiscale model captures the magnitude of the shear strains as well as the overall topology of the persistent shear band.

Finally, these results are encouraging from the point of view of amalgamating advanced experimental results with multiscale computations to extract material behavior accurately.

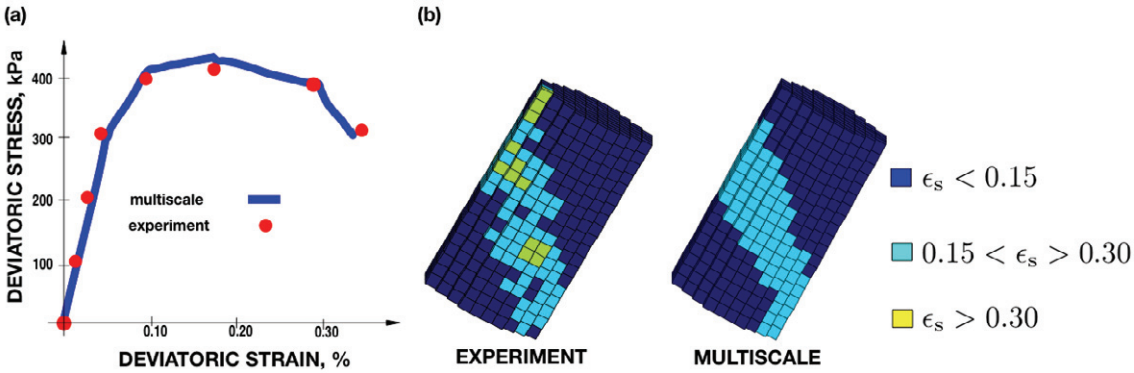

Fig. 8. (a) Global average deviatoric stress versus global average deviatoric strain from hierarchical multiscale computations compared against the experimental response. (b) Deviatoric strain map across the cylindrical sample at deformation stage 7 corresponding to a nominal axial strain around 0.13. The reader is referred to [8] for more information regarding multicell computations.

Closure

We have described a hierarchical multiscale procedure capable of reproducing the essential mechanical features of granular materials under shear loading. Both numerical and physical experiments were used to verify and validate the proposed method. The crux of the method is the extraction of two central plastic internal variables: friction and dilatancy. These are used in a simple elastoplastic model similar to a nonassociative Drucker–Prager. The multiscale technique extracts the plastic internal variables from the micro-structure directly and hence bypasses phenomenological evolution laws, typically invoked in modeling. Simulations based on underlying discrete mechanics (represented by the discrete element method) showed the potential of the procedure to extract information accurately from any discrete mechanics model. On the other hand, the computations based on advanced experimental data from 3D-DIC and X-ray CT, showed the ability of the model to extract real material behavior from complex three-dimensional micro-structures. In particular, a persisting shear band was observed in the experiment and accurately captured by the multiscale model. This is the first time that advanced experimentation and multiscale models are amalgamated, rendering more powerful and predictive multiscale models. These results may open the door to more physics-based constitutive models for complex engineering materials in the future.

References

[1] Liu, W.K., Karpov, E.G., Park, H.S., 2006. Nano Mechanics and Materials. John Wiley & Sons Ltd., Chichester, West Sussex, UK.

[2] Tadmor, E., Ortiz, M., Phillips, R., 1996. Quasicontinuum analysis of defects in solids. Philosophical Magazine A 73, 1529–1563.

[3] Belytschko, T., Loehnert, S., Song, J.-H., 2008. Multiscale aggregating discontinuities: a method for circumventing loss of material stability. International Journal for Numerical Methods in Engineering 73, 869-894.

[4] Dascalu, C., Cambou, B., 2008. Multiscale approaches to geomaterials. Acta Geotechnica 3.

[5] Wellmann, C., Lillie, C., Wriggers, P., 2007. Homogenization of granular material modeled by a three-dimensional discrete element method. Computers and Geotechnics 35, 394–405.

[6] Nitka, M., Bilbie, B., Combe, G., Dascalu, C., Desrues, J., 2009. A micro–macro (DEM–FEM) model of the behavior of granular solids. In: 1st International Symposium on Computational Geomechanics (ComGeo I), Juan-les-Pins, France, pp. 38–48.

[7] Andrade, J.E., Tu, X., 2009. Multiscale framework for behavior prediction in granular media. Mechanics of Materials 41, 652–669.

[8] Andrade, J.E., Avila, C.F., Hall, S.A., Lenoir, N., and Viggiani, G., 2011. Multiscale modeling and characterization of granular matter: From grain kinematics to continuum mechanics. Journal of the Mechanics and Physics of Solids 59, 237-250
[9] Muir Wood, D., 2004. Geotechnical Modelling. Spon Press, Taylor & Francis Group, London.
[10] Belytschko, T., Liu, W.K., Moran, B., 2000. Nonlinear Finite Elements for Continua and Structures. John Wiley & Sons Ltd, West Sussex, UK.
[11] H ughes, T.J.R., 1987. The Finite Element Method. Prentice-Hall, Englewood Cliffs, NJ.
[12] Cundall, P.A., Strack, O.D.L., 1979. A discrete numerical model for granular assemblies. Ge´otechnique 29, 47–65.
[13] Desai, C.S., Siriwardane, H.J., 1984. Constitutive Laws for Engineering Materials. Prentice-Hall, Inc.
[14] Andrade, J.E., Borja, R.I., 2006. Capturing strain localization in dense sands with random density. International Journal for Numerical Methods in Engineering 67, 1531–1564.
[15] Baz˘ant, Z.P., Caner, F.C., Carol, I., Adley, M.D., Akers, S.A., 2000. Microplane model M4 for concrete. I: formulation with work-conjugate deviatoric stress.
Journal of Engineering Mechanics 126, 944–953.
[16] Dafalias, Y.F., Popov, E.P., 1975. A model of nonlinearly hardening materials for complex loadings. Acta Mechanica 21, 173–192.
[17] DiMaggio, F.L., Sandler, I.S., 1971. Material model for granular soils. Journal of the Engineering Mechanics Division-ASCE 97, 935–950.
[18] Grueschow, E., Rudnicki, J.W., 2005. Elliptic yield cap constitutive modeling for high porosity sandstone. International Journal of Solids and Structures 42 (16–17), 4574–4587.
[19] Vermeer, P.A., de Borst, R., 1984. Non-associated plasticity for soils, concrete and rock. Heron 29, 1–62.
[20] Desrues, J., Chambon, R., Mokni, M., Mazerolle, F., 1996. Void ratio evolution inside shear bands in triaxial sand specimens studied by computed tomography. Geotechnique 46, 527–546.
[21] Oda, M., Takemura, T., Takahashi, M., 2004. Microstructure in shear band observed by microfocus X-ray computed tomography. Ge´ otechnique 54, 539–542.
[22] Rechenmacher, A.L., 2006. Grain-scale processes governing shear band initiation and evolution in sands. Journal of the Mechanics and Physics of Solids 54, 22–45.
[23] Santamarina, J.C., 2001. Soils and Waves. John Wiley & Sons Ltd., New York.
[24] Bardet, J.P., Proubet, J., 1991. Adaptive dynamic relaxation for statics of granular materials. Computers & Structures 39, 221–229.
[25] Ng, T.T., 2009. Shear strength and micro-descriptors of bidisperse ellipsoids under different loading paths. Mechanics of Materials 41, 748–763.
[26] Rothenburg, L., Bathurst, R.J., 1989. Analytical study of induced anisotropy in idealized granular materials. Ge´otechnique 39, 601–614.
[27] Tu, X., Andrade, J.E., 2008. Criteria for static equilibrium in particulate mechanics computations. International Journal for Numerical Methods in Engineering 75, 1581–1606.
[28] Muir Wood, D., 1990. Soil Behaviour and Critical State Soil Mechanics. Cambridge University Press, Cambridge, UK.
[29] Reynolds, O., 1885. On the dilatancy of media composed of rigid particles in contact. Philosophical Magazine and Journal of Science 20, 468–481.
[30] Hall, S.A., Bornert, M., Desrues, J., Pannier, Y., Lenoir, N., Viggiani, G., Besuelle, P., 2010. Discrete and continuum analysis of localized deformation in sand using X-ray micro CT and volumetric digital image correlation. Ge´otechnique 60, 315–322.
[31] Chang, C.S., Hicher, P.Y., 2004. An elastic-plastic model for granular materials with microstructural considerations. International Journal of Solid and Structures 42, 4258-4277.
[32] Nicot, F., Darve, F., 2005. A multiscale approach to granular materials. Mechanics of Material 37, 980-1006.
[33] Cundall, P.A., 2001. A discontinuous future for numerical modelling in geomechanics? Geotechnical Engineering ICE 149, 41–47.
[34] Christoffersen, J., Mehrabadi, M.M., Nemat-Nasser, S., 1981. A micromechanical description of granular material behavior. Journal of Applied Mechanics 48, 339–344.
[35] Barber, B., David, D., Hannu, H., 1996. The quick algorithm for convex hulls. ACM Transactions of Mathematical Software 22, 469–483.

[36] Lenoir, N., Bornert, M., Desrues, J., Be´suelle, P., Viggiani, G., 2007. 3D digital image correlation applied to X-ray microtomography images from triaxial compression tests on argillaceous rock. Strain 43, 193–205.
[37] Schofield, A., Wroth, P., 1968. Critical State Soil Mechanics. McGraw-Hill, New York.
[38] Fish, J., Belytschko, T., 2008. A First Course in Finite Elements. John Wiley & Sons Ltd., Chichester, West Sussex, UK.